J Nanopart Res (2014) 16:2750
DOI 10.1007/s11051-014-2750-2

RESEARCH PAPER

Alcohol solvents evaporation-induced self-assembly synthesis of mesoporous $TiO_{2-x-y}C_xN_y$ nanoparticles toward visible-light driven photocatalytic activity

Shou-Heng Liu · Han-Ren Syu · Chung-Yi Wu

Received: 14 July 2014 / Accepted: 12 November 2014 / Published online: 22 November 2014

Abstract A one-step solvent evaporation-induced self-assembly (SEISA) process was demonstrated to prepare carbon and nitrogen co-doping mesoporous TiO_2 nanoparticles (MesoTi$O_{2-x-y}C_xN_y$-*S*) using an ionic liquid as carbon and nitrogen sources as well as mesoporous template. After the evaporation of different solvents (methanol, ethanol, and isopropanol) and subsequent calcinations at 773 K, the obtained MesoTi$O_{2-x-y}C_xN_y$-*S* samples were systematically characterized by a variety of spectroscopic and analytical techniques, including small- and large-angle X-ray diffraction (XRD), Raman, transmission electron microscopy (TEM), N_2 adsorption–desorption isotherms, Fourier transform infrared (FTIR), and X-ray photoelectron (XPS) spectroscopies. The results indicate that the solvents play an essential role on the chemical microstructure, doping elemental states, and photocatalytic performance of catalysts. The MesoTi$O_{2-x-y}C_xN_y$-I samples have the lowest band gap of ca. 2.75 eV and strongest absorbance of visible light in the range of 400–600 nm. Among the MesoTi$O_{2-x-y}C_xN_y$-*S* photocatalysts, the MesoTi$O_{2-x-y}C_xN_y$-M catalysts show superior photocatalytic activity of hydrogen generation in methanol aqueous solution under visible light irradiation as compared to MesoTi$O_{2-x-y}C_xN_y$-E, MesoTi$O_{2-x-y}C_xN_y$-I, and commercial Degussa TiO_2. This result could be attributed to the moderate C,N co-doping amounts on their developed mesoporous texture (pore size = 8.0 nm) and high surface area (107 $m^2\ g^{-1}$) of TiO_2 (crystallite size = 9.9 nm) in the MesoTi$O_{2-x-y}C_xN_y$-M catalysts.

Keywords Solvent evaporation-induced self-assembly · Mesoporous titania · $TiO_{2\text{-}x\text{-}y}C_xN_y$ · Ionic liquid · Photocatalytic

Introduction

In the recent years, much effort has been devoted to modification of TiO_2 in order to allow the utilization of a wider fraction of visible light (Ould-Chikh et al. 2014; Venieri et al. 2014; Zhang et al. 2014). Until now, the adjusting of the electronic structure of TiO_2 materials is an effective approach, for example, substituting lattice oxygen with nonmetal elements such as C, N, S, F, Cl, or I (Han et al. 2014; Huang and Wey 2013; Umadevi et al. 2014; Vereb et al. 2013; Wang et al. 2009). It was reported that co-doped TiO_2 with two or more nonmetal elements, such as C–N (Cong et al. 2006; Dolat et al. 2012; Ruzybayev and Shah 2014; Wang and Lim 2011; Wu and Ju 2014; Xu et al. 2011; Yang et al. 2008; Zhang and Song 2009), S–N (Todorova et al. 2013), N–F (Chen et al. 2009)

S.-H. Liu (✉) · H.-R. Syu · C.-Y. Wu
Department of Chemical and Materials Engineering,
National Kaohsiung University of Applied Sciences,
Kaohsiung 80778, Taiwan
e-mail: shliu@kuas.edu.tw

and C–S (Scarisoreanu et al. 2014) can further exhibit synergistic effect of increasing the visible-light activities. Among them, C and N co-doping onto TiO_2 has shown to have superior photocatalytic performance under visible light (Chen et al. 2007a) because of its large specific surface area and developed porosity favors solar energy conversion. In the earlier reports, C,N co-doping can be attained by mechano-chemical, ammonolysis, and sputtering processes (Hojamberdiev et al. 2012; Noguchi et al. 2005; Yin et al. 2007). These methods may be performed at a high temperature which can unavoidably destruct the mesoporosity of the mesoporous TiO_2, lead to phase transition and lower their photocatalytic performance. To keep their developed porosity, a lot of low temperature processes, such as sol–gel (Xu et al. 2011), hydrothermal, and solvothermal methods (Cong et al. 2006; Dolat et al. 2012; Wang and Lim 2011) have been proposed for preparing mesoporous TiO_2. Among these techniques, hydrolysis, nitriding, and crystallization processes were controlled by the mixture of solvent, surfactant template, and chemical sources of Ti, C, and N, which can determine the mesoporosity of the mesoporous TiO_2.

Solvent evaporation-induced self-assembly (SEISA) has been reported to be a good method to synthesize mesoporous TiO_2 thin films (Martínez-Ferrero et al. 2007) because it is easy to handle the synthesis system (solvents, surfactant templates, and Ti precursors). In addition, the possible recycle of evaporated solvent makes it an environmental friendly synthetic route to scale up. The SEISA was proven to be successful in preparation of N-doped mesoporous TiO_2 thin films by postnitriding mesoporous TiO_2 photoelectrodes (Martínez-Ferrero et al. 2007; Soni et al. 2008). However, limited studies were found in the synthesis of C and N co-doped mesoporous TiO_2 powders using SEISA process.

Ionic liquids (ILs) have many distinctive properties, including negligible vapor pressures, superior thermal stability, tunable solubility for both organic and inorganic molecules, and much synthetic flexibility (Dupont and Scholten 2010; Ma et al. 2010). Recently, the utilization of ILs in synthesis of metal nanoparticles, supported catalysts and functional material composites has been widely investigated. Also, ILs used as the templates for micro and mesostructured materials have been regarded as a promising substitute for structural directing agents in nanocasting. For example, various ILs such as $[C_4mim][PF_6]$, $[C_4mim][BF_4]$, $[C_4mim][CF_3SO_3]$, and $[C_6mim][PF_6]$ have been employed as the templates for the preparation of mesoporous TiO_2 (Chen et al. 2007b; Han et al. 2010; Li et al. 2014; Sajjad et al. 2013) that not only had a high surface area but also a controllable pore size distribution, which improved the photoactivities. In the previous work (Liu and Syu 2013), we reported a facile procedure to synthesize C,N co-doped mesoporous TiO_2 nanoparticles using an IL as carbon, nitrogen sources, and mesoporous templates. In this work, to further study the solvent effects on the developed mesoporosity of C,N co-doped TiO_2 during SEISA process, a certain amounts of ILs (1-Ethyl-3-methylimidazolium chloride, EMIC) was added into various alcohol solutions (methanol, ethanol, and isopropanol) of titanium (IV) isopropoxide under continuous stirring, followed by treating a SEISA process and calcinations at 773 K. The resulting $\mathrm{MesoTiO}_{2-x-y}\mathrm{C}_x\mathrm{N}_y\text{-}S$ materials were characterized by various spectroscopic and analytical techniques. The effects of different alcohols on the SEISA synthesis of mesostructured C,N co-doped TiO_2 nanoparticles were evaluated by photocatalytic activities in water splitting using visible light.

Experimental method

Photocatalysts preparation

First, ca. 3.0 g of 1-Ethyl-3-methylimidazolium chloride (EMIC, Sigma) were added in a 40 mL of various solvents (methanol, ethanol, and isopropanol), followed by adding 3.4 g of 35 wt% hydrochloric acid and continuously stirring until dissolution. Second, ca. 4 mL water containing 1.2 g citric acid was added into the above solution under vigorous stirring for 2 h at room temperature. Consequently, 5.6 g titanium (IV) isopropoxide (TTIP, ACROS) was dissolved into 40 mL of respective solvents (methanol, ethanol, and isopropanol) and then slowly added to the above solution. The mixture solution was performed with the SEISA technique at 343 K for 48 h to attain the solid product. Finally, the resultant solid was heated to 773 K with a heating rate of 1 K min^{-1} and maintained at the same temperature for 5 h under the air flow to remove template. The obtained C,N co-doped mesoporous TiO_2 nanoparticles were denoted as

MesoTi$O_{2-x-y}C_xN_y$-*S* where *S* represents the different solvents mentioned above.

Characterization methods

To identify the crystallite size and phase of samples, the powder X-ray diffraction (XRD) patterns were obtained with a PANalytical (X'Pert PRO) instrument using Cu-Kα radiation ($\lambda = 0.1541$ nm) in a 2θ range of 20–80°. Raman measurements were operated with a Lambda Dimension-P2 spectrometer coupled with a microscope in a reflectance mode using a 785 nm excitation laser source and a spectral resolution of 0.3 cm^{-1}. Small-angle X-ray scattering (SAXS) of all samples was measured on a Nanostar U system (Bruker, AXS Gmbh). The high-resolution transmission electron microscopy (TEM) images were performed on an electron microscope (JEOL TEM-3010) with an electron acceleration voltage of 200 kV. Nitrogen adsorption isotherms were conducted at 77 K using a Micromeritics ASAP 2020 system and the corresponding specific surface areas were calculated from nitrogen adsorption data in the relative pressure (P/P_0) range from 0.05 to 0.2 via Brunauer-Emmett-Teller (BET) equation. The pore volumes and pore size distribution curves were derived from the adsorption branch using Barrett-Joyner-Halenda (BJH) model. Fourier transform infrared (FTIR) spectra were obtained on a Bio-rad 165 spectrometer with 4 cm^{-1} resolution using KBr pellets at room temperature. X-ray photoelectron spectra (XPS) were collected on a spectrometer (PHI 5000 VersaProbe) in an ultrahigh vacuum condition (10^{-10} Torr) at room temperature. The binding energies in XPS spectra for the synthesized samples have been referenced to the C 1 s core level at 284.5 eV of adventitious carbon. A JASCO V-670 UV–vis spectrometer with an integrating sphere apparatus was used to record UV–vis diffuse reflectance spectra of samples.

Photocatalytic measurements

The photocatalytic activities of photocatalysts were examined in terms of hydrogen production from water splitting under visible light irradiation. The reaction was carried out in a top-irradiation photoreactor with an optical Quartz window (Liu and Syu 2012). Briefly, ca. 0.2 g photocatalyst was dispersed homogeneously with a magnetic stirrer in 155 mL of aqueous solution containing 40 mL methanol in the reaction vessel. Prior to the irradiation, the suspension was purged with extra pure argon to remove air. Then, the solution was illuminated by a 450 W Xe lamp (Newport, Model 66142) with a cut-off filter ($\lambda \geq 420$ nm) under continuously magnetic stirring. The temperature of the whole reactor was kept at 298 K with a circulation of cold water. The hydrogen evolution was frequently measured by online gas chromatography (Bruker 430-GC) equipped with a thermal conductivity detector (TCD) and a packed column (molecular sieve 5A, 99.999 % N_2 carrier).

Results and discussion

As shown in Fig. 1, the large-angle XRD patterns of the MesoTi$O_{2-x-y}C_xN_y$-*S* samples all indicated well-resolved peaks at $2\theta = 25.3°$, 37.9°, 48.3°, 53.9°, 55.2°, 62.9°, 69.1°, 70.3°, and 75.2°, respectively, which are the features of (101), (004), (200), (105), (211), (204), (116), (220), and (215) diffraction peaks.

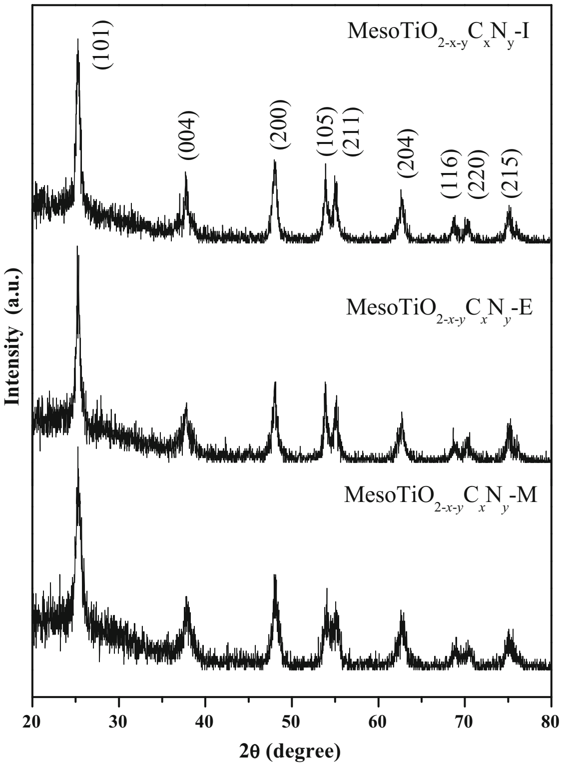

Fig. 1 Large-angle XRD patterns of MesoTi$O_{2-x-y}C_xN_y$-*S* samples

This indicates the existence of well crystalline anatase phase (JCPDS, CAS number 21-1272) of all TiO_2 nanoparticles without phase transition after heat treatments. As can be seen in Table 1, the crystallite sizes (d_p) of all samples were calculated using Scherrer formula based on (101) diffraction peak. It was observed that the d_p was in the order of MesoTi$O_{2-x-y}C_xN_y$-I > MesoTi$O_{2-x-y}C_xN_y$-E > MesoTi$O_{2-x-y}C_xN_y$-M, which implied that the solvents with shorter alcohol chain lengths could hinder the grain growth. Additionally, the intensity of diffraction peak (101) of MesoTi$O_{2-x-y}C_xN_y$-M samples was found to be slightly decreased, indicating the restricted crystallization of TiO_2 nanoparticles affected by methanol in the SEISA synthesis. Additional Raman spectroscopy displayed in Fig. 2 was used to further confirm the crystalline phase of TiO_2. Six Raman peaks were observed for MesoTi$O_{2-x-y}C_xN_y$-*S* samples at 144 cm^{-1} (E_g), 197 cm^{-1} (E_g), 399 cm^{-1} (B_{1g}), 513 cm^{-1} (A_{1g}), 519 cm^{-1} (B_{1g}), and 639 cm^{-1} (E_g), suggesting the pure anatase phase of TiO_2 which is in accordance with the XRD results. Also, a slight shift toward high wavenumber region and broadening of E_g bands at 144 cm^{-1} are observed for MesoTi$O_{2-x-y}C_xN_y$-M while methanol was used as solvent during SEISA process, which may be due to the formation of oxygen deficiency (Parker and Siegel 1990) and small particle size (Yang et al. 2010) of TiO_2 nanoparticles. This finding is consistent with the above-mentioned XRD results.

The small-angle powder X-ray scattering patterns (see Fig. 3) of MesoTi$O_{2-x-y}C_xN_y$-M, MesoTi$O_{2-x-y}C_xN_y$-E and MesoTi$O_{2-x-y}C_xN_y$-I samples show only one feature at 2θ ≒ 0.35°, 0.20°, and 0.25°, indicating the existence of wormlike mesopores with maximum distribution of the nearest-neighbor particle-center-to-particle-center distances of 25.2, 44.1, and 35.3 nm,

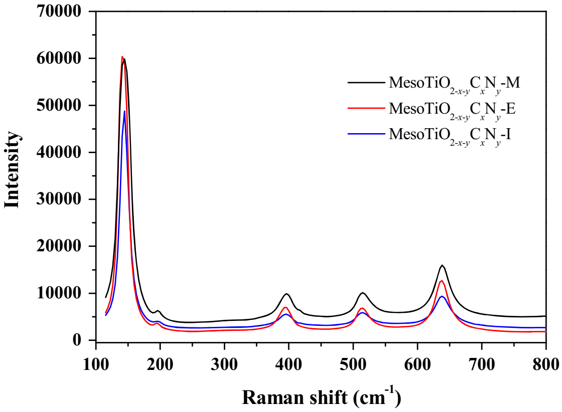

Fig. 2 Raman spectra of MesoTi$O_{2-x-y}C_xN_y$-*S* samples

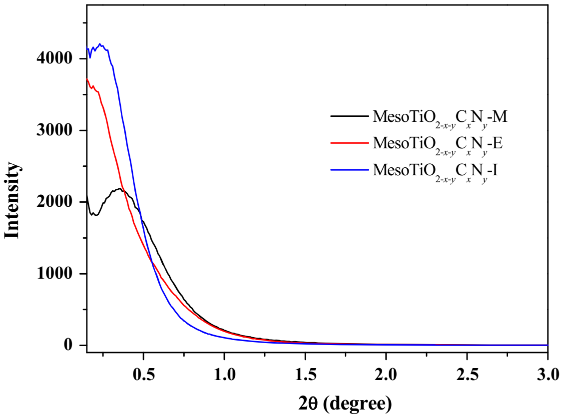

Fig. 3 Small-angle XRD patterns of MesoTi$O_{2-x-y}C_xN_y$-*S* samples

Table 1 Textural properties of MesoTi$O_{2-x-y}C_xN_y$-*S* samples

Sample	S_{BET} (m^2g^{-1})[a]	D_{BJH} (nm)[b]	V_{tot} (cm^3g^{-1})[c]	d_p (nm)[d]	N (at%)[e]	C (at%)[f]	BG (eV)[g]
MesoTi$O_{2-x-y}C_xN_y$-M	107	8.0	0.16	9.9	3.1	4.5	3.02
MesoTi$O_{2-x-y}C_xN_y$-E	76	8.0	0.13	15.9	3.8	5.4	2.94
MesoTi$O_{2-x-y}C_xN_y$-I	56	10.0	0.11	20.3	4.8	6.6	2.75

[a] BET surface area

[b] BJH pore diameter

[c] Total pore volume

[d] Average crystallite size deduced by the Scherrer formula based on the (101) diffraction peak in Fig. 1

[e] N contents analyzed by XPS

[f] C contents (excluded adventitious carbon) analyzed by XPS

[g] Band gap

respectively. Among all the MesoTi$O_{2-x-y}C_xN_y$-*S* samples, MesoTi$O_{2-x-y}C_xN_y$-M possesses the obvious diffraction peak. However, the weaker and unclear peaks can be observed for MesoTi$O_{2-x-y}C_xN_y$-E and MesoTi$O_{2-x-y}C_xN_y$-I, indicating the less ordering of mesoporous structure was formed upon the presence of ethanol and isopropanol during SEISA. This result implies that the degree of self-assembly may be affected by the solvents existing in synthetic mixture.

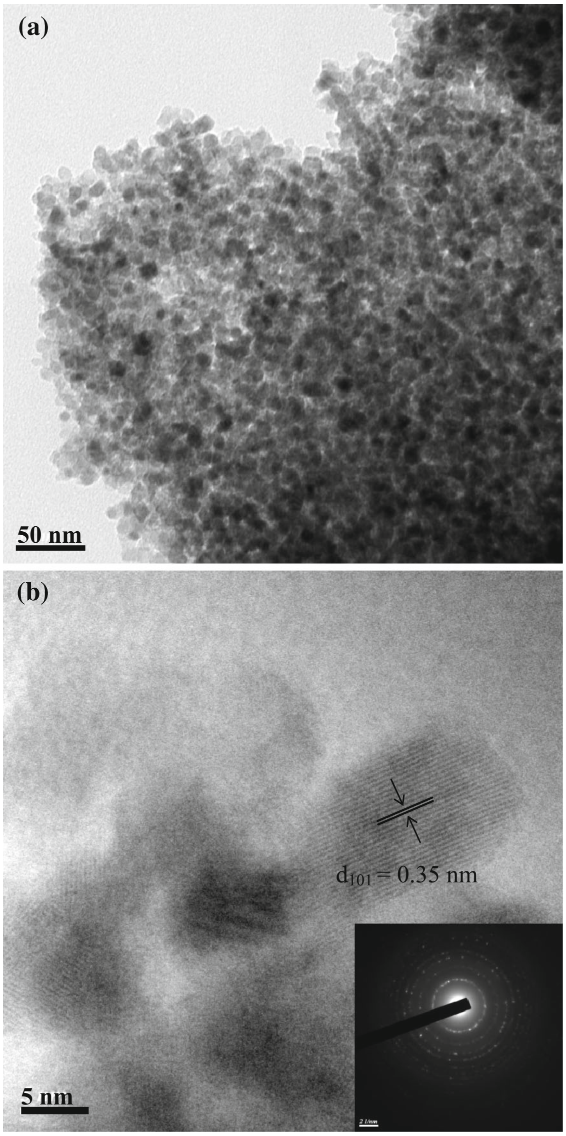

Fig. 4 **a** Low magnification, **b** high magnification TEM images of MesoTi$O_{2-x-y}C_xN_y$-M samples. *Inset* corresponding selected area electron diffraction pattern

As displayed in Fig. 4a, the representative TEM images of MesoTi$O_{2-x-y}C_xN_y$-M show low and high electron density regions throughout the samples which are due to the formation of TiO_2 nanoparticles in a mesoscopic disordering during SEISA. A similar result (Sivaranjani and Gopinath 2011) was reported previously that the wormhole-like mesoporosity of N-doped TiO_2 synthesized via solution combustion method was observed. The mesoporous structures formed in the inter-nanoparticles would increase the light scattering inside the pore channels and thus enhance the light harvesting (Pan et al. 2008). Moreover, the high-resolution TEM image in Fig. 4b indicates that the majority of lattice fringes are attributed to (101) plane, i.e., $d_{101} \fallingdotseq 0.35$ nm of anatase phase, in agreement with the result obtained from XRD and Raman analysis. As can be seen in the inset of Fig. 4b, selected area electron diffraction (SAED) pattern of the MesoTi$O_{2-x-y}C_xN_y$-M demonstrates well-resolved diffuse electron diffraction rings with their respective d-spacings of (101), (004), (200), (211), (204), (220), and (215), again in a good accordance with the anatase phase of spherical TiO_2 nanocrystals (JCPDS, CAS number 21-1272).

Figure 5a shows the N_2 adsorption–desorption isotherms of MesoTi$O_{2\text{-}x\text{-}y}C_xN_y$-*S* samples. According to the IUPAC classification, all the samples are type-IV isotherms with well-developed hysteresis loops, implying the typical signatures of mesoporosity. Additionally, large uniform mesopores with a cage-like pore structure connected by small size windows are observed in these samples (Das et al. 2009) since

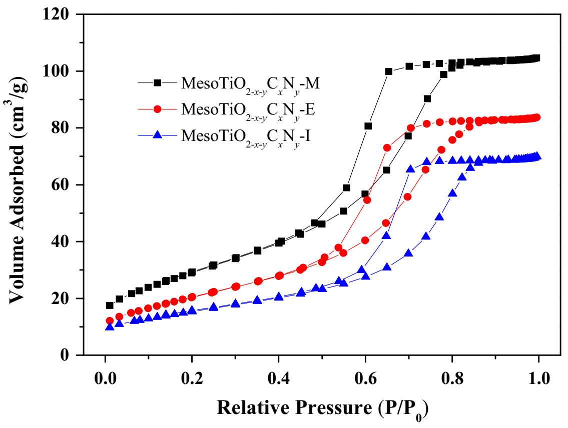

Fig. 5 N_2 adsorption/desorption isotherm of MesoTiO_{2-x-y} C_xN_y-*S* samples

the loop in the P/P$_0$ range of 0.4–0.9 is an intermediate between typical H1 and H2-type hysteresis. Compared with MesoTiO$_{2-x-y}$C$_x$N$_y$-M, the hysteresis loops of MesoTiO$_{2-x-y}$C$_x$N$_y$-E, and MesoTiO$_{2-x-y}$C$_x$N$_y$-I, the shifting to the region of higher relative pressure suggests the increasing pore sizes. The pore size distributions determined from adsorption branches of isotherms by the BJH method of the MesoTiO$_{2-x-y}$C$_x$N$_y$-*S* are shown in Fig. 6. The pore sizes ranges of MesoTiO$_{2-x-y}$C$_x$N$_y$-M and MesoTiO$_{2-x-y}$C$_x$N$_y$-E samples are between 3 to 10 nm, indicating the narrow distributions of the mesopores. Nonetheless, the broad distribution of pore range is observed for MesoTiO$_{2-x-y}$C$_x$N$_y$-I, suggesting the perturbation of mesoporous ordering upon the usage of isopropanol during SEISA. The properties of MesoTiO$_{2-x-y}$C$_x$N$_y$-*S* samples obtained from N$_2$ adsorption–desorption isotherms such as BET surface area, pore volume, and pore size are summarized in Table 1. The MesoTiO$_{2-x-y}$C$_x$N$_y$-M samples were found to possess BET surface areas of ca. 107 m^2 g^{-1} and a uniform pore size distribution of 8.0 nm. The much lower sorption curves and the broader pore size distribution were observed for MesoTiO$_{2-x-y}$C$_x$N$_y$-E and MesoTiO$_{2-x-y}$C$_x$N$_y$-I, resulting in their lower surface areas (ca. 76 and 56 m^2 g^{-1}, respectively, in Table 1) and pore volumes, which may be caused by the more disorder mesostructures and larger crystallite size (d_p), while the samples were prepared from ethanol and isopropanol solvents during SEISA.

The FTIR spectra of the MesoTiO$_{2-x-y}$C$_x$N$_y$-*S* are shown in Fig. 7. The broad peaks observed at ca. 3,000–3,700 and 1,640 cm^{-1} could be attributed to surface adsorbed water and hydroxyl groups; a major factor influencing the photocatalytic activity (Ding et al. 2000) which is generally motivated by hydroxyl radicals produced via the step involving the attack of photogenerated holes on surface bound water or hydroxyl groups (Dhananjeyan et al. 2000). A weak feature at ca. 1,400 cm^{-1} could be attributed to the CO or NH$_4^+$ groups which imply that carbon and nitrogen were successfully incorporated into the structural lattice (Xu et al. 2010). The signals in the range of 500–1,250 cm^{-1} are characteristic of the formation of O–Ti–O lattices (Chen et al. 2005). In addition, two peaks at 2,920 and 2,851 cm^{-1} corresponding to asymmetric and symmetric C–H stretching vibrations, respectively, were observed in the MesoTiO$_{2-x-y}$C$_x$N$_y$-*S* samples.

The chemical states of carbon and nitrogen atoms doped in the MesoTiO$_{2-x-y}$C$_x$N$_y$-*S* samples were examined by XPS analysis. The high-resolution C 1 s XPS spectra of MesoTiO$_{2-x-y}$C$_x$N$_y$-*S* are shown in Fig. 8. All the MesoTiO$_{2-x-y}$C$_x$N$_y$-*S* samples possess a peak at 284.5 eV which is attributed to the presence

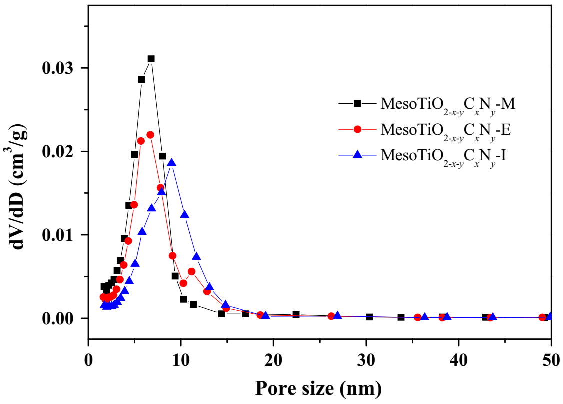

Fig. 6 The BJH pore size distribution of MesoTiO$_{2-x-y}$C$_x$N$_y$-*S* samples

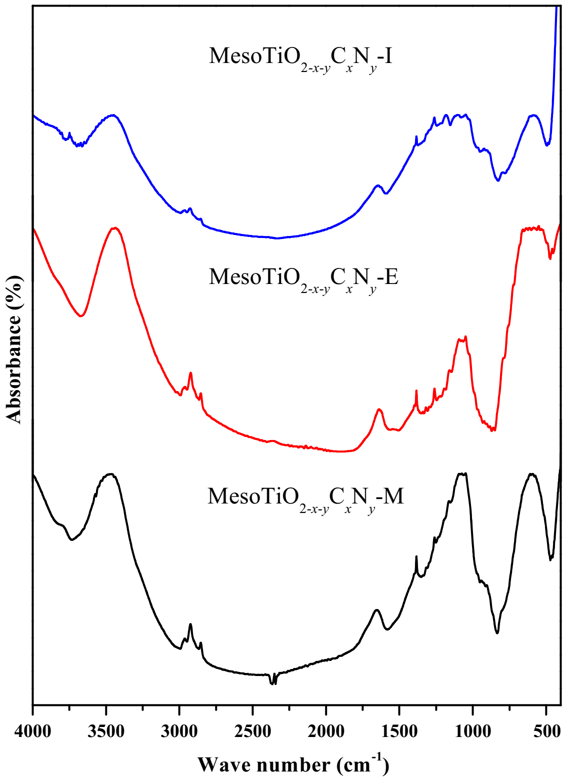

Fig. 7 FTIR spectra of various MesoTiO$_{2-x-y}$C$_x$N$_y$-*S* samples

of adventitious carbon. An additional peak at ca. 285.7 eV which can be ascribed to C–O bonds was observed in MesoTiO$_{2-x-y}$C$_x$N$_y$-*S*, indicating that carbonated species may be formed or carbon atoms may substitute titania atoms in the form of Ti–O-C bonds on the TiO$_2$ surface (Song et al. 2013; Zhao et al. 2010). Moreover, the MesoTiO$_{2-x-y}$C$_x$N$_y$-I sample has the highest contents of carbon (6.6 at%, see Table 1) doped in the titania surface among the MesoTiO$_{2-x-y}$C$_x$N$_y$-*S*. Based on the earlier reports (Wang et al. 2012; Zhao et al. 2010), formation of carbonated species on TiO$_2$ surface might act as the photosensitizer to improve the visible-light absorption ability. It is worth to note that the peak at ca. 281 eV from Ti–C bonds was not found, suggesting that carbon atoms may not replace O atoms in the TiO$_2$ lattice.

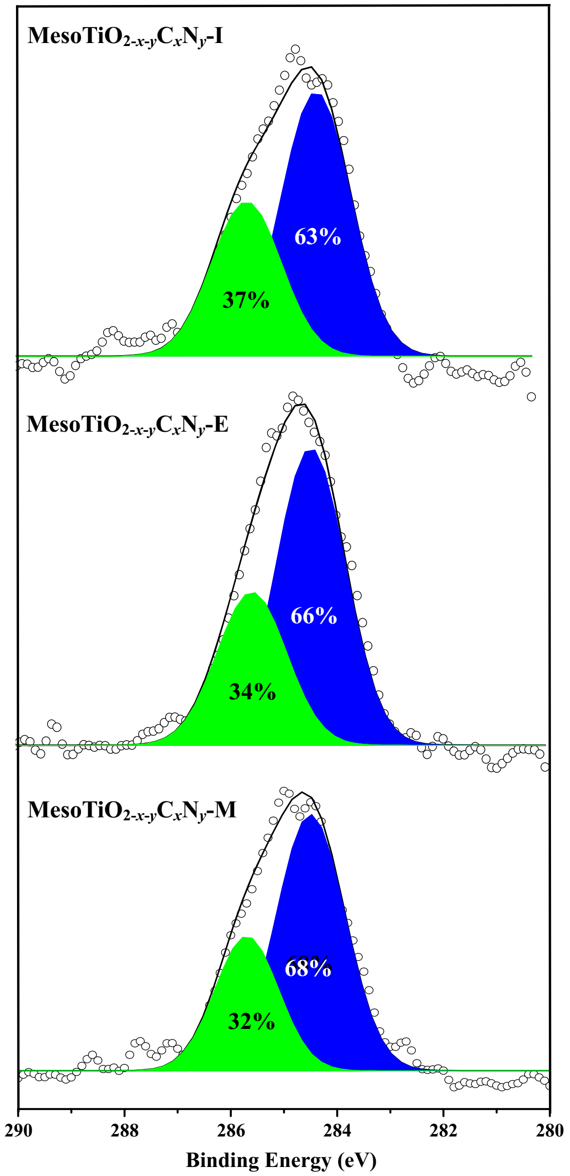

Fig. 8 XPS spectra of MesoTiO$_{2-x-y}$C$_x$N$_y$-*S* at the C 1 s region

Furthermore, the states of N doped on Meso TiO$_{2-x-y}$C$_x$N$_y$-*S* samples were studied using high-resolution and curve-fitting of N 1 s XPS spectra, as shown in Fig. 9. A broad peak ranging from 396 to 402 eV was observed in the MesoTiO$_{2-x-y}$C$_x$N$_y$-*S* at N 1 s region. For the MesoTiO$_{2-x-y}$C$_x$N$_y$-*S* samples, the overlay of two deconvoluted peaks at 398.4 and 400.2 eV was observed, indicating no formation of N–Ti–N bonds (396 eV) by replacement of the oxygen atoms in the TiO$_2$ crystal lattice (Manole et al. 2014). The N 1 s peaks at 398.4 eV can be attributed to the anionic N$^-$ in the O–Ti–N linkages (Etacheri et al. 2010), as the electronegativity of N atoms is smaller than O atoms, the electron density around N is decreased as compared to that in a TiN crystal. However, the N 1 s peak at 400.2 eV can be ascribed to oxidized nitrogen, such as Ti–O–N or Ti–N–O linkages in the MesoTiO$_{2-x-y}$C$_x$N$_y$-*S* samples (Etacheri et al. 2010; Naik et al. 2011). In addition, the weak feature at 402.2 eV has been known to represent molecular adsorbed N species (Tian et al. 2010). From XPS analysis, the corresponding percentages of N dopants are estimated to be 3.1–4.8 at%, which were successfully doped on MesoTiO$_{2-x-y}$C$_x$N$_y$-*S* samples, as indicated in Table 1. UV–vis diffuse reflectance (UV–vis DR) spectra of commercial TiO$_2$ (P25) and MesoTiO$_{2-x-y}$C$_x$N$_y$-*S* samples are shown in Fig. 10a. It can be seen that a broad background absorption in the visible light region is observed for MesoTiO$_{2-x-y}$C$_x$N$_y$-M, which is not present in the case of P25. Upon using ethanol and isopropanol as solvents during SEISA, further increases in the intensity of visible light can be found. In addition, MesoTiO$_{2-x-y}$C$_x$N$_y$-*S* samples possess a remarkable red-shift absorbance threshold as compared to P25, implying that the increased visible-light absorption edges and intensities of MesoTiO$_{2-x-y}$C$_x$N$_y$-*S* can be due to the synergistic effect of carbon and nitrogen species co-doped on the TiO$_2$ (Chen et al. 2007a). The plot of $(\alpha h\nu)^2$ vs. the energy of the absorbed light (Fig. 10b) can be used to evaluate the band gaps of the synthetic samples which are indirect semiconductors. As a result, their

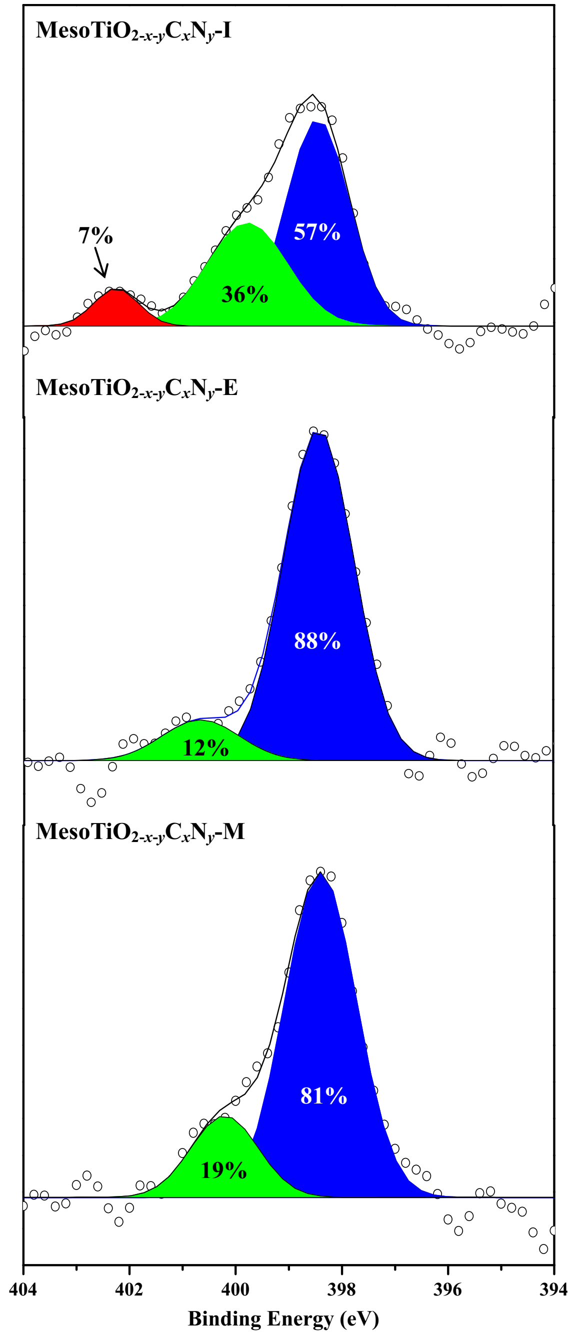

Fig. 9 XPS spectra of MesoTiO$_{2-x-y}$C$_x$N$_y$-S at the N 1 s region

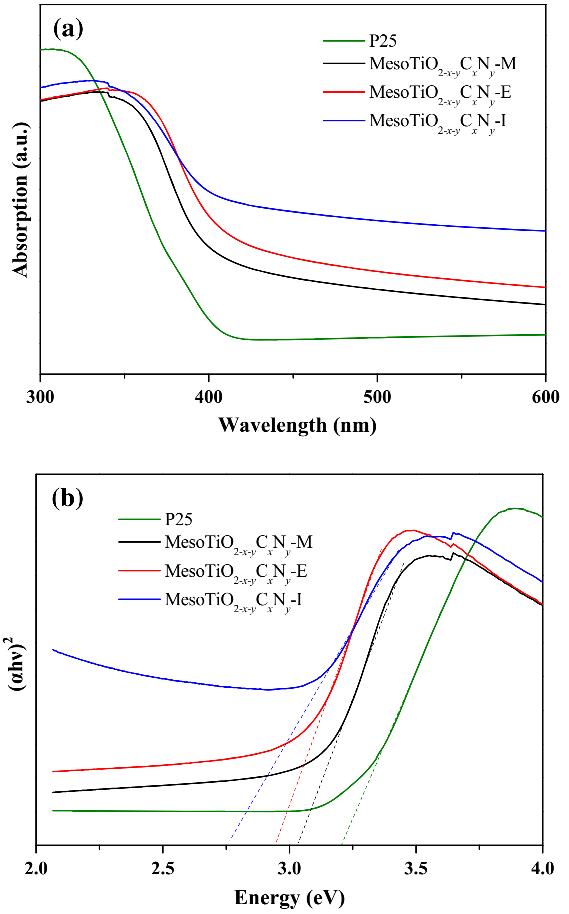

Fig. 10 **a** DR UV–vis spectra and **b** band gap evaluation from the plots of $(\alpha h\nu)^2$ vs. the energy of the absorbed light for P25 and MesoTiO$_{2-x-y}$C$_x$N$_y$-S samples

corresponding energy band gaps are obtained and summarized in Table 1. All the MesoTiO$_{2-x-y}$C$_x$N$_y$-S samples have lower band gap energies as compared to that of P25 (ca. 3.2 eV). Among them, the MesoTiO$_{2-x-y}$C$_x$N$_y$-I samples are found to have the lowest band gap of ca. 2.75 eV and strongest absorbance of visible light in the range of 400–600 nm, which are favorable for the photocatalytic evolution of hydrogen under visible light. This finding indicates that more carbon and nitrogen atoms could be doped into the lattice of titania and thus leads to the higher visible-light response, while the isopropanol was used during SEISA.

The visible-light responsive activities of P25 and various MesoTiO$_{2-x-y}$C$_x$N$_y$-S catalysts were evaluated by photocatalytic evolution of hydrogen from suspension of catalysts in aqueous methanol solution. In general, photocatalytic activity of TiO$_2$ can be affected by various factors such as specific surface area, crystal size, crystallinity, pore and phase structures, surface properties, and band gap values (Das et al. 2010; Kim and Kang 2012). The previous results (Das et al. 2010; Ouzzine et al. 2014) indicated that higher surface area of TiO_2 improves the absorption of more water molecules on the surface and the higher crystalline but smaller particle size results in an efficient utilization of charge carriers, while the photogenerated carriers diffuse rapidly to the surface and reacts quickly with the adsorbed water molecules. As can be seen in Fig. 11, the H_2 generation amounts of P25 and $MesoTiO_{2-x-y}C_xN_y$-*S* increase with increasing irradiation time. The photocatalytic activities of $MesoTiO_{2-x-y}C_xN_y$-*S* are highly enhanced while compared to commercial Degussa TiO_2 (P25) which is due to the little absorption in the visible light and low surface area. Among all the $MesoTiO_{2-x-y}C_xN_y$-*S* examined, the $MesoTiO_{2-x-y}C_xN_y$-M catalysts prepared with methanol as solvents during SEISA, which have distinctive properties including relatively high surface areas (107 $m^2\ g^{-1}$, see Table 1), smaller crystallite size (9.9 nm, see Table 1), mesoporous structure, and pure anatase crystalline phase, were found to exhibit the superior visible-light photocatalytic activity. The most evident red shift (see Fig. 10) caused by C,N co-doping is observed for Meso $TiO_{2-x-y}C_xN_y$-I catalyst which has the worst photocatalytic performance among the $MesoTiO_{2-x-y}C_xN_y$-*S*. This finding implies that the absorbance of visible-light in the $MesoTiO_{2-x-y}C_xN_y$-*S* could not be the dominant factor for H_2 evolution from water splitting. From the results discussed above, C,N atoms co-doped on TiO_2 with mesoporous structure and high surface area is responsible for surpassing photocatalytic activity under visible light.

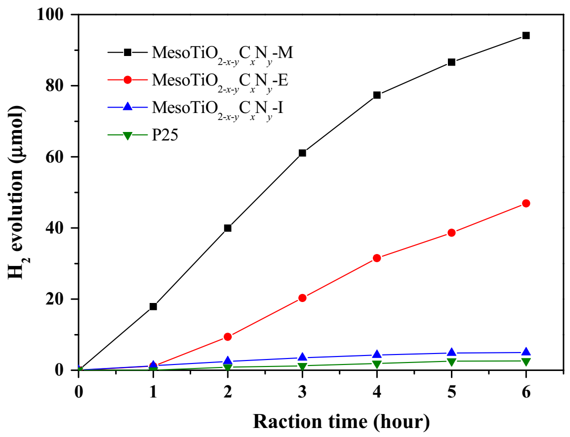

Fig. 11 Photocatalytic H_2 evolution as a function of time catalyzed by $MesoTiO_{2-x-y}C_xN_y$-*S* and commercial P25 photocatalysts

Conclusions

In a conclusion, C,N co-doped on mesostructured photocatalysts synthesized via a simple SEISA method with different kinds of solvents was proposed. The resultant $MesoTiO_{2-x-y}C_xN_y$-*S* samples were thoroughly characterized by a variety of spectroscopic and analytical techniques and subsequently used as photocatalysts for hydrogen evolution from water splitting under visible light. Although $MesoTiO_{2-x-y}C_xN_y$-*S* photocatalysts (S = E and I) have stronger absorption of visible light in the region of 400–600 nm, photocatalytic generation of hydrogen (78.4 $\mu mol\ g^{-1}\ h^{-1}$) for $MesoTiO_{2-x-y}C_xN_y$-M was highly enhanced over those of $MesoTiO_{2-x-y}C_xN_y$-E, $MesoTiO_{2-x-y}C_xN_y$-I and the commercial P25. This improvement of visible-light-responsive (>420 nm) photocatalysis in the splitting of water may be due to the suitable C,N co-doping on well-developed mesoporous architecture with large surface area (107 $m^2\ g^{-1}$), which is almost double that of the $MesoTiO_{2-x-y}C_xN_y$-I.

Acknowledgments The support of this work by the National Science Council, Taiwan is gratefully acknowledged.

References

Chen X, Lou Y, Samia ACS, Burda C, Gole JL (2005) Formation of oxynitride as the photocatalytic enhancing site in nitrogen-doped titania nanocatalysts: Comparison to a commercial nanopowder. Adv Funct Mater 15:41–49. doi:10.1002/adfm.200400184

Chen DM, Jiang ZY, Geng JQ, Wang Q, Yang D (2007a) Carbon and nitrogen co-doped TiO_2 with enhanced visible-light photocatalytic activity. Ind Eng Chem Res 46:2741–2746. doi:10.1021/ie061491k

Chen SY, Han CC, Tsai CH, Huang J, Chen-Yang YW (2007b) Effect of morphological properties of ionic liquid-templated mesoporous anatase TiO_2 on performance of PEMFC with Nafion/TiO_2 composite membrane at elevated temperature and low relative humidity. J Power Sources 171:363–372. doi:10.1016/j.jpowsour.2007.06.047

Chen DM, Jiang ZY, Geng JQ, Zhu JH, Yang D (2009) A facile method to synthesize nitrogen and fluorine co-doped TiO_2 nanoparticles by pyrolysis of $(NH_4)_2TiF_6$. J Nanoparticle Res 11:303–313. doi:10.1007/s11051-008-9383-2

Cong Y, Chen F, Zhang J, Anpo M (2006) Carbon and nitrogen-codoped TiO_2 with high visible light photocatalytic activity. Chem Lett 35:800–801. doi:10.1246/cl.2006.800

Das SK, Bhunia MK, Sinha AK, Bhaumik A (2009) Self-assembled mesoporous zirconia and sulfated zirconia nanoparticles synthesized by triblock copolymer as template. J Phys Chem C 113:8918–8923. doi:10.1021/jp9014096

Das SK, Bhunia MK, Bhaumik A (2010) Self-assembled TiO_2 nanoparticles: mesoporosity, optical and catalytic properties. Dalton Trans 39(2010):4382–4390. doi:10.1039/c000317d

Dhananjeyan MR, Kandavelu V, Renganathan R (2000) A study on the photocatalytic reactions of TiO_2 with certain pyrimidine bases: effects of dopants (Fe^{3+}) and calcination. J Mol Catal A Chem 151:217–223. doi:10.1016/S1381-1169(99)00246-0

Ding Z, Lu GQ, Greenfield PF (2000) Role of the crystallite phase of TiO_2 in heterogeneous photocatalysis for phenol oxidation in water. J Phys Chem B 104:4815–4820. doi:10.1021/jp993819b

Dolat D, Quici N, Kusiak-Nejman E, Morawski AW, Puma GL (2012) One-step, hydrothermal synthesis of nitrogen, carbon co-doped titanium dioxide (N, C-TiO2) photocatalysts. Effect of alcohol degree and chain length as carbon dopant precursors on photocatalytic activity and catalyst deactivation. Appl Catal B Environ 115–116:81–89. doi:10.1016/j.apcatb.2011.12.007

Dupont J, Scholten JD (2010) On the structural and surface properties of transition-metal nanoparticles in ionic liquids. Chem Soc Rev 39:1780–1804. doi:10.1039/b822551f

Etacheri V, Seery MK, Hinder SJ, Pillai SC (2010) Highly visible light active $TiO_{2\text{-}x}N_x$ heterojunction photocatalysts. Chem Mater 22:3843–3853. doi:10.1021/cm903260f

Han CC, Lin YP, Ho SY, Lai YC, Chen SY, Huang J, Chen-Yang YW (2010) Effect of ionic liquid-templated mesoporous anatase TiO_2 on performance of dye-sensitized solar cell. J Phys D Appl Phys 43:035102. doi:10.1088/0022-3727/43/3/035102

Han CS, Andersen J, Likodimos V, Falaras P, Linkugel J, Dionysiou DD (2014) The effect of solvent in the sol-gel synthesis of visible light-activated, sulfur-doped TiO_2 nanostructured porous films for water treatment. Catal Today 224:132–139. doi:10.1016/j.cattod.2013.11.052

Hojamberdiev M, Prasad RM, Morita K, Zhu YF, Schiavon M, Al Gurlo, Riedel R (2012) Template-free synthesis of polymer-derived mesoporous SiOC/TiO_2 and SiOC/N-doped TiO_2 ceramic composites for application in the removal of organic dyes from contaminated water. Appl Catal B Environ 115:303–313. doi:10.1016/j.apcatb.2011.12.036

Huang B, Wey MY (2013) Characterization of N-doped TiO_2 nanoparticles supported on $SrTiO_3$ via a sol-gel process. J Nanoparticle Res 16:2178. doi:10.1007/s11051-013-2178-0

Kim J, Kang M (2012) High photocatalytic hydrogen production over the band gap-tuned urchin-like Bi_2S_3-loaded TiO_2 composites system. Int J Hydrogen Energy 37:8249–8256. doi:10.1016/j.ijhydene.2012.02.057

Li FT, Wang XJ, Zhao Y, Liu JX, Hao YJ, Liu RH, Zhao DS (2014) Ionic-liquid-assisted synthesis of high-visible-light-activated N-B-F-tri-doped mesoporous TiO_2 via a microwave route. Appl Catal B Environ 144:442–453. doi:10.1016/j.apcatb.2013.07.050

Liu S-H, Syu H-R (2012) One-step fabrication of N-doped mesoporous TiO_2 nanoparticles by self-assembly for photocatalytic water splitting under visible light. Appl Energy 100:148–154. doi:10.1016/j.apenergy.2012.03.063

Liu S-H, Syu H-R (2013) High visible-light photocatalytic hydrogen evolution of C, N-codoped mesoporous TiO2 nanoparticles prepared via an ionic-liquid template approach. Int J Hydrogen Energy 38:13856–13865. doi:10.1016/j.ijhydene.2013.08.094

Ma Z, Yu JH, Dai S (2010) Preparation of inorganic materials using ionic liquids. Adv Mater 22:261–285. doi:10.1002/adma.200900603

Manole AV, Dobromir M, Apetrei R, Nica V, Luca D (2014) Surface characterization of sputtered N:TiO_2 thin films within a wide range of dopant concentration. Ceram Int 40:9989–9995. doi:10.1016/j.ceramint.2014.02.097

Martínez-Ferrero E, Sakatani Y, Boissière C, Grosso D, Fuertes A, Fraxedas J, Sanchez C (2007) Nanostructured titanium oxynitride porous thin films as efficient visible-active photocatalysts. Adv Funct Mater 17:3348–3354. doi:10.1002/adfm.200700396

Naik B, Martha S, Parida KM (2011) Facile fabrication of Bi_2O_3/$TiO_{2\text{-}x}N_x$ nanocomposites for excellent visible light driven photocatalytic hydrogen evolution. Int J Hydrogen Energy 36:2794–2802. doi:10.1016/j.ijhydene.2010.11.104

Noguchi D, Kawamata Y, Nagatomo T (2005) The response of TiO_2 photocatalysts codoped with nitrogen and carbon to visible light. J Electrochem Soc 152:D124–D129. doi:10.1149/1.1990581

Ould-Chikh S, Proux O, Afanasiev P, Khrouz L, Hedhili MN, Anjum DH, Harb M, Geantet C, Basset JM, Puzenat E (2014) Photocatalysis with chromium-doped TiO_2: bulk and surface doping. ChemSusChem 7:1361–1371. doi:10.1002/cssc.201300922

Ouzzine M, Maciá-Agulló JA, Lillo-Ródenas MA, Quijada C, Linares-Solano A (2014) Synthesis of high surface area TiO_2 nanoparticles by mild acid treatment with HCl or HI for photocatalytic propene oxidation. Appl Catal B Environ 154–155:285–293. doi:10.1016/j.apcatb.2014.02.039

Pan JH, Zhang XW, Du AJ, Sun DD, Leckie JO (2008) Self-etching reconstruction of hierarchically mesoporous F-TiO_2 hollow microspherical photocatalyst for concurrent membrane water purifications. J Am Chem Soc 130:11256–11257. doi:10.1021/ja803582m

Parker JC, Siegel RW (1990) Calibration of the Raman spectrum to the oxygen stoichiometry of nanophase TiO_2. Appl Phys Lett 57:943–945

Ruzybayev I, Shah SI (2014) The role of oxygen pressure in nitrogen and carbon co-doped TiO_2 thin films prepared by pulsed laser deposition method. Surf Coat Technol 241:148–153. doi:10.1016/j.surfcoat.2013.10.073

Sajjad S, Leghari SAK, Zhang JL (2013) Copper impregnated ionic liquid assisted mesoporous titania: visible light photocatalyst. RSC Adv 3:12678–12687. doi:10.1039/c3ra23347b

Scarisoreanu M, Morjan I, Alexandrescu R, Fleaca CT, Badoi A, Dutu E, Niculescu A-M, Luculescu C, Vasile E, Wang J, Bouhadoun S, Herlin-Boime N (2014) Enhancing the visible light absorption of titania nanoparticles by S and C doping in a single-step process. Appl Surf Sci 4:5880–5886. doi:10.1016/j.apsusc.2014.01.135

Sivaranjani K, Gopinath CS (2011) Porosity driven photocatalytic activity of wormhole mesoporous $TiO_{2-x}N_x$ in direct sunlight. J Mater Chem 21:2639–2647. doi:10.1039/c0jm03825c

Song JJ, Zhu BL, Zhao WL, Hu XJ, Shi YK, Huang WP (2013) Characterization and photocatalytic properties of Ru, C co-modified one-dimensional TiO_2-based composites prepared via a single precursor approach. J Nanopart Res 15:1494. doi:10.1007/s11051-013-1494-8

Soni SS, Henderson MJ, Bardeau JF, Gibaud A (2008) Visible-light photocatalysis in titania-based mesoporous thin films. Adv Mater 20:1493–1498. doi:10.1002/adma.200701066

Tian HJ, Hu LH, Zhang CN, Liu WQ, Huang Y, Mo L, Guo L, Sheng J, Dai SY (2010) Retarded charge recombination in dye-sensitized nitrogen-doped TiO_2 solar cells. J Phys Chem C 114:1627–1632. doi:10.1021/jp9103646

Todorova N, Vaimakis T, Petrakis D, Hishita S, Boukos N, Giannakopoulou T, Giannouri M, Antiohos S, Papageorgiou D, Chaniotakis E, Trapalis C (2013) N and N, S-doped TiO_2 photocatalysts and their activity in NO_x oxidation. Catal Today 209:41–46. doi:10.1016/j.cattod.2012.11.019

Umadevi M, Parimaladevi R, Sangari M (2014) Synthesis, characterization and photocatalytic activity of fluorine doped TiO_2 nanoflakes synthesized using solid state reaction method. Spectrochim Acta A 120:365–369. doi:10.1016/j.saa.2013.10.046

Venieri D, Fraggedaki A, Kostadima M, Chatzisymeon E, Binas V, Zachopoulos A, Kiriakidis G, Mantzavinos D (2014) Solar light and metal-doped TiO_2 to eliminate water-transmitted bacterial pathogens: Photocatalyst characterization and disinfection performance. Appl Catal B Environ 154:93–101. doi:10.1016/j.apcatb.2011.12.007

Vereb G, Manczinger L, Oszko A, Sienkiewicz A, Forro L, Mogyorosi K, Dombi A, Hernadi K (2013) Highly efficient bacteria inactivation and phenol degradation by visible light irradiated iodine doped TiO_2. Appl Catal B Environ 129:194–201. doi:10.1016/j.apcatb.2012.08.037

Wang XP, Lim TT (2011) Effect of hexamethylenetetramine on the visible-light photocatalytic activity of C-N codoped TiO_2 for bisphenol A degradation: evaluation of photocatalytic mechanism and solution toxicity. Appl Catal A Gen 399:233–241. doi:10.1016/j.apcata.2011.04.002

Wang Q, Jiang ZY, Wang YB, Chen DM, Yang D (2009) Photocatalytic properties of porous C-doped TiO_2 and Ag/C-doped TiO_2 nanomaterials by eggshell membrane templating. J Nanoparticle Res 11:375–384. doi:10.1007/s11051-008-9390-3

Wang DH, Jia L, Wu XL, Lu LQ, Xu AW (2012) One-step hydrothermal synthesis of N-doped TiO_2/C nanocomposites with high visible light photocatalytic activity. Nanoscale 4:576–584. doi:10.1039/c1nr11353d

Wu Y-C, Ju L-S (2014) Annealing-free synthesis of C-N co-doped TiO_2 hierarchical spheres by using amine agents via microwave-assisted solvothermal method and their photocatalytic activities. J Alloys Compd 604:164–170. doi:10.1016/j.jallcom.2014.03.023

Xu QC, Wellia DV, Amal R, Liao DW, Loo JSC, Tan TTY (2010) Superhydrophilicity-assisted preparation of transparent and visible light activated N-doped titania film. Nanoscale 2:1122–1127. doi:10.1039/c0nr00105h

Xu QC, Wellia DV, Yan S, Liao DW, Lim TM, Tan TTY (2011) Enhanced photocatalytic activity of C-N-codoped TiO_2 films prepared via an organic-free approach. J Hazar Mater 188:172–180. doi:10.1016/j.jhazmat.2011.01.088

Yang X, Cao C, Erickson L, Hohn K, Maghirang R, Klabunde K (2008) Synthesis of visible-light-active TiO_2-based photocatalysts by carbon and nitrogen doping. J Catal 260:128–133. doi:10.1016/j.jcat.2008.09.016

Yang GD, Jiang Z, Shi HH, Xiao TC, Yan ZF (2010) Preparation of highly visible-light active N-doped TiO_2 photocatalyst. J Mater Chem 20:5301–5309. doi:10.1039/c0jm00376j

Yin S, Komatsu M, Zhang Q, Saito F, Sato T (2007) Synthesis of visible-light responsive nitrogen/carbon doped titania photocatalyst by mechanochemical doping. J Mater Sci 42:2399–2404. doi:10.1007/s10853-006-1231-0

Zhang SJ, Song LM (2009) Preparation of visible-light-active carbon and nitrogen codoped titanium dioxide photocatalysts with the assistance of aniline. Catal Commun 10:1725–1729. doi:10.1016/j.catcom.2009.05.017

Zhang K, Wang XD, Guo XL, He TO, Feng YM (2014) Preparation of highly visible light active Fe-N co-doped mesoporous TiO_2 photocatalyst by fast sol-gel method. J Nanopart Res 16:2246. doi:10.1007/s11051-014-2246-0

Zhao L, Chen XF, Wang XC, Zhang YJ, Wei W, Sun YH, Antonietti M, Titirici MM (2010) One-step solvothermal synthesis of a carbon@TiO_2 dyade structure effectively promoting visible-light photocatalysis. Adv Mater 22:3317–3321. doi:10.1002/adma.201000660